

A Hybrid Numerical Method to Compute Erythrocyte TMP in Low-Frequency Electric Fields

Changjun Liu*, Dongwoo Sheen, and Kama Huang

Abstract—This paper presents a coupling method of the finite element method and the boundary element method to compute the transmembrane potential (TMP) of an erythrocyte in a low-frequency electric field. We compute an *in vitro* erythrocyte's TMP induced by external electric fields by this hybrid method. It takes advantage of the homogeneous characteristics from both intracellular region and extracellular region. Moreover, we may use a fine three-dimensional (3-D) mesh around the thin membrane and avoid 3-D meshes in other regions. Numerical results of a spherical cell show that the hybrid method is accurate. The computed threshold of the applied electric field for membrane electric breakdown agrees well with those experimental results. Numerical results can also guide us to locate the maximum induced TMP on the erythrocyte membrane in various electric fields. Some further applications of the hybrid method are also discussed.

Index Terms—Boundary element method (BEM), erythrocyte, finite element method (FEM), membrane, transmembrane potential (TMP).

I. INTRODUCTION

THE transmembrane potential (TMP) of a cell varies while it is in applied electric fields. The TMP induced by external electric fields has been studied in electroporation, electrofusion, and electromagnetic bioeffects [1]–[3]. There are several methods to calculate the TMP variation. One approach is to use the analytic method, which usually assumes that a cell's shape is regular, such as an ellipsoid or a sphere. Thus, it is an estimation of the induced TMP on real cells. Another method is to use the finite element method (FEM) with a better cell model to achieve more accurate results [4]–[6]. The FEM has been widely applied to solving Maxwell equations [7], [8], since it is stable and good at modeling complex structures. However, it needs special efforts to build a nonuniform mesh for a cell with a very thin membrane. Because the ratio between cell diameter and membrane thickness is above 1000, it is not easy to achieve a good three-dimensional (3-D) mesh.

The boundary element method (BEM) is suitable for homogeneous media, and can model regions with rapidly changing variables with better accuracy than the FEM [9], [10]. Meanwhile,

Manuscript received December 23, 2002; revised March 18, 2003. This work was supported by the KOSEF APEC postdoctoral scholarship, KOSEF Grant No. 2000-1-10300-001-5, and NSFC Grant No. 60125102. Asterisk indicates corresponding author.

*C. Liu is with the Department of Radio-Electronics, College of Electronics and Information Science, Sichuan University, Chengdu 610064, China (e-mail: cqliu@scu.edu.cn).

D. Sheen is with the Department of Mathematics, Seoul National University, Seoul 151-747, Korea (e-mail: sheen@snu.ac.kr)

K. Huang is with the College of Electronics and Information Science, Sichuan University, Chengdu 610064, China (e-mail: kmhuang@scu.edu.cn).

Digital Object Identifier 10.1109/TNB.2003.813933

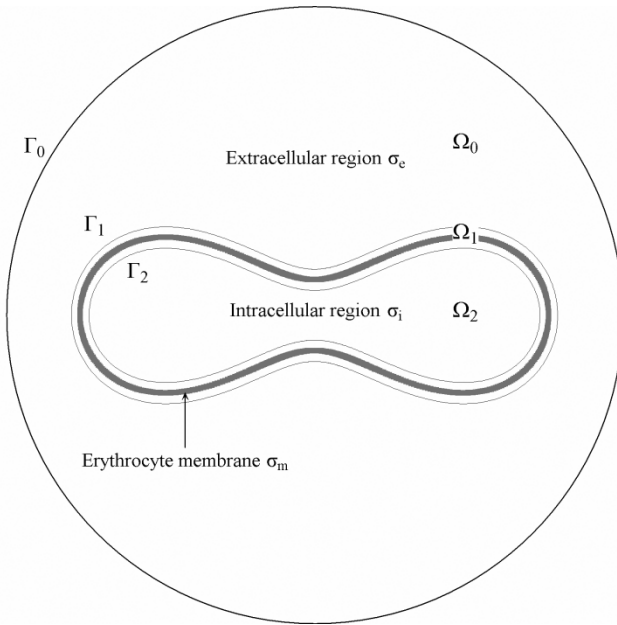


Fig. 1. Configuration of domains and boundaries. Norm directions of each boundary are defined as outward norm directions in all domains.

meshes are only on the boundaries, i.e., a two-dimensional surface boundary for a closed 3-D region. Thus, it is easier to obtain meshes for the BEM than for the FEM. An FEM–BEM coupling method has been introduced and studied in [11] and [12]. The coupling method has been applied to dealing with unbounded electromagnetic problems to take advantages of both the FEM and the BEM.

The induced TMP of cells in applied electric fields attracted several researchers' efforts [5], [6]. In this paper, we compute the induced TMP of a human erythrocyte. Since both intracellular and extracellular regions are homogeneous, the BEM is applied. The FEM is applied to the inhomogeneous region around the membrane. Then, the FEM and BEM are coupled together to find electric fields distribution around it. In Section II, theory and the erythrocyte model are presented. The hybrid numerical method is shown in Section III. In Section IV, the hybrid method is verified, and some numerical results are shown. In the last section, some applications of this method are discussed.

II. THEORY AND MODEL

When human erythrocytes are far from each other in an isosmotic solution, we may pick out one for computation. We choose a spherical surface Γ_0 to contain one erythrocyte at the center, and denote the inside region by Ω , as shown in Fig. 1. The gray region represents the membrane, and its surfaces are

conformably extended to Γ_1 and Γ_2 . Designate regions between Γ_0 and Γ_1 , between Γ_1 and Γ_2 , and inside Γ_2 by Ω_0 , Ω_1 , and Ω_2 , respectively. We denote the conductivities of intracellular region, membrane, and extracellular region by σ_i , σ_m , and σ_e , respectively. In this paper, we make two assumptions: 1) erythrocytes are far from each other and 2) both intracellular and extracellular regions are homogeneous.

A. Theory

An electric field $\mathbf{E}(\omega t)$ applied to the solution can induce a current $\mathbf{J}(\omega t)$. If the frequency ω is significantly low compared to the relaxational frequency of the erythrocyte, we may neglect the displacement current and treat \mathbf{E} as a quasi-static field and \mathbf{J} as a steady current.

Thus, when Γ_0 is imposed with a Dirichlet boundary condition, we may write the problem as

$$\begin{cases} -\nabla \cdot (\sigma \nabla \phi) = 0, & \text{in } \Omega \\ \phi = f, & \text{on } \Gamma_0 \end{cases} \quad (1)$$

where σ and ϕ are the conductivity and potential, respectively.

Since it is homogeneous in Ω_0 and Ω_2 , (1) is facilitated to the Laplace equation in these regions. Notice that the potential ϕ and the normal current $J_n = \sigma(\partial\phi/\partial n)$ are continuous on Γ_1 and Γ_2 . If conductivities are constant around Γ_1 and Γ_2 , the normal derivative of potential $\partial\phi/\partial n$ is also continuous. We can rewrite (1) as

$$\begin{cases} -\nabla^2 \phi = 0, & \text{in } \Omega_0, \Omega_2 \\ -\nabla \cdot (\sigma \nabla \phi) = 0, & \text{in } \Omega_1 \\ \phi^- = \phi^+, & \text{on } \Gamma_1, \Gamma_2 \\ \frac{\partial \phi^-}{\partial n} = \frac{\partial \phi^+}{\partial n}, & \text{on } \Gamma_1, \Gamma_2 \\ \phi = f, & \text{on } \Gamma_0 \end{cases} \quad (2)$$

where ϕ_j^- and ϕ_j^+ are potentials of the inner and outer surfaces of boundary Γ_j , respectively. Therefore, the BEM is applied to Ω_0 and Ω_2 while the FEM is applied to Ω_1 so as to solve (2), which is equivalent to (1).

B. Erythrocyte

A so-called degree-4 equation in Cartesian coordinates is used to describe the surface of a human biconcave erythrocyte [7]

$$(x^2 + y^2 + z^2)^2 + P(x^2 + y^2) + Qz^2 + R = 0 \quad (3)$$

where $P = -1.53 \times 10^{-11}$ m, $Q = 4.20 \times 10^{-11}$ m, and $R = -1.06 \times 10^{-23}$ m². To represent an erythrocyte surface, (3) is much accurate than the Cassini equation, which contains two adjustable parameters. Fig. 2 shows a cross section of the surface defined by (3), where the membrane thickness is 7 nm.

We take $\sigma_i = 0.8$ S/m and $\sigma_m = 5 \times 10^{-5}$ S/m for the conductivities of the intracellular region and of the erythrocyte membrane [13], [14]. The conductivity of the extracellular region σ_e varies in different kinds of *in vivo* experiments. Hence, we change the extracellular conductivity in this paper to find how it influences the induced TMP.

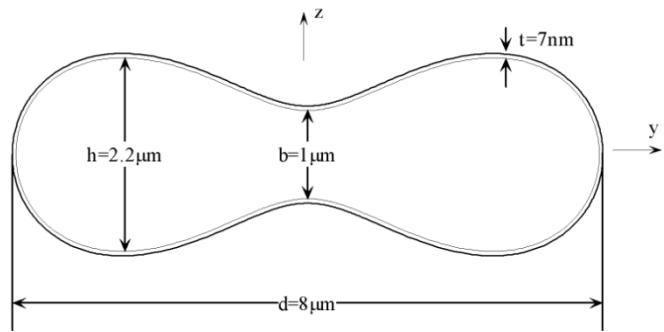


Fig. 2. Cross section of a human erythrocyte. The short axis denotes the direction of an erythrocyte, i.e., \mathbf{z} . (Membrane thickness is magnified.).

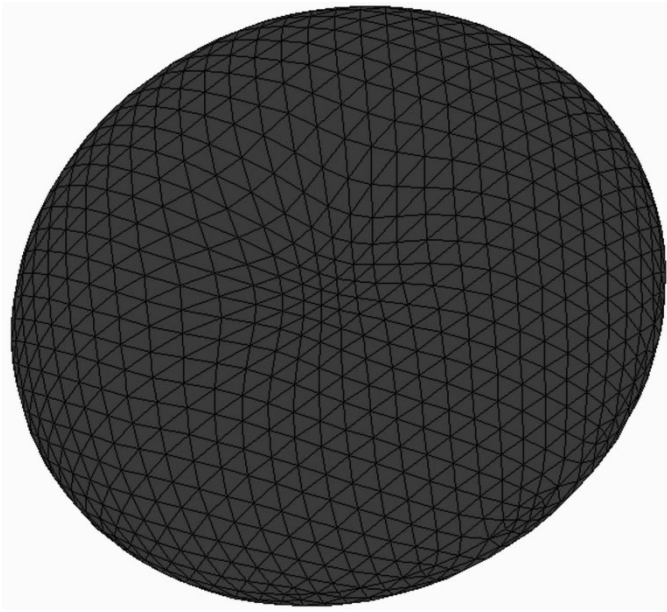


Fig. 3. Mesh on an erythrocyte surface.

C. Mesh Generation

A mapping technique is used to transform a regular triangular mesh on a plane to the surface Γ_2 . The mesh quality is improved by moving each node to the center of its neighbors. A mesh of Γ_2 , which is conforming to the erythrocyte surface defined by (3), is shown in Fig. 3. This curved surface mesh is applied to the 3-D BEM later. Denote this mesh as layer 1, which represents the boundary Γ_2 . Move all N_L nodes of layer 1 by distance d_m along its outward norm direction to achieve a conforming layer, layer 2. Then, layer by layer, we can get M layers, where the M^{th} layer presents boundary Γ_1 . Denote by $N_{\text{FEM}} (= M \times N_L)$ the number of nodes inside Ω_1 , and number them from 1 to N_{FEM} . By connecting the nodes of the i^{th} layer with the corresponding nodes of the $(i+1)^{\text{th}}$ layer, we obtain a 3-D prismatic mesh, which is applied to the 3-D FEM. For the spherical boundary Γ_0 , we use a similar mapping technique to generate a triangular mesh with N_B nodes on it, and number them from $N_{\text{FEM}} + 1$ to $N_{\text{FEM}} + N_B$. Thus, triangular meshes are on surfaces Γ_0 , Γ_1 , and Γ_2 , and the prismatic mesh of N_{FEM} nodes is in the region Ω_1 .

III. METHODS

Linear elements are used for both the FEM in Ω_1 and the BEM in Ω_0 and Ω_2 . Then we perform a FEM–BEM coupling on Γ_1 and Γ_2 to solve (2). Hereafter, we present a scheme for the FEM and BEM used here and describe the FEM–BEM coupling method.

A. The FEM

Consider the problem restricted to Ω_1 with the Neumann boundary conditions on Γ_1 and Γ_2

$$\begin{cases} -\nabla \cdot (\sigma \nabla \phi) = 0, & \text{in } \Omega_1 \\ \sigma \frac{\partial \phi}{\partial n} = g_1, & \text{on } \Gamma_1 \\ -\sigma \frac{\partial \phi}{\partial n} = g_2, & \text{on } \Gamma_2 \end{cases}. \quad (4)$$

We denote the electric potential at the i th node by Φ_i at all nodes. Then, a standard FEM yields the following system of linear equations:

$$[A] \{\Phi\} = \{b\} \quad (5)$$

where $[A]$ is an $N_{\text{FEM}} \times N_{\text{FEM}}$ sparse matrix, and $\{\Phi\}$ and $\{b\}$ are two $N_{\text{FEM}} \times 1$ vectors. We separate all nodes in Ω_1 into three groups, and rewrite (5) in the corresponding form

$$\begin{bmatrix} A_{aa} & A_{ab} & A_{ac} \\ A_{ba} & A_{bb} & A_{bc} \\ A_{ca} & A_{cb} & A_{cc} \end{bmatrix} \begin{Bmatrix} \Phi^a \\ \Phi^b \\ \Phi^c \end{Bmatrix} = \begin{Bmatrix} [T_2] \left\{ \frac{\partial \Phi^a}{\partial n} \right\} \\ 0 \\ -[T_1] \left\{ \frac{\partial \Phi^c}{\partial n} \right\} \end{Bmatrix} \quad (6)$$

where $\{\Phi^a\}$ and $\{\Phi^c\}$ are two $N_L \times 1$ vectors approximating the potentials at nodes on Γ_2 and Γ_1 , $\{\Phi^b\}$ is an $M \times N_L - 2N_L$ vector approximating the potentials at nodes between Γ_1 and Γ_2 , and $\{T_1\}$ and $\{T_2\}$ are two $N_L \times N_L$ sparse matrices.

B. The BEM

In Ω_0 and Ω_2 , we propose to solve the Laplace equations with Dirichlet boundary conditions. These two problems from (2) are

$$\begin{cases} -\nabla^2 \phi = 0, & \text{in } \Omega_0 \\ \phi = f, & \text{on } \Gamma_0 \\ \phi = f_1, & \text{on } \Gamma_1 \end{cases} \quad (7a)$$

and

$$\begin{cases} -\nabla^2 \phi = 0, & \text{in } \Omega_2 \\ \phi = f_2, & \text{on } \Gamma_2 \end{cases} \quad (7b)$$

where f , f_1 , and f_2 are the potentials at Γ_0 , Γ_1 , and Γ_2 , respectively. From the regular direct BEM, in Ω_0 and Ω_2 , we obtain the system of linear equations

$$[G_1] \begin{Bmatrix} -\frac{\partial \Phi^c}{\partial n} \\ \frac{\partial \Phi^d}{\partial n} \end{Bmatrix} = [H_1] \begin{Bmatrix} \Phi^c \\ \Phi^d \end{Bmatrix} \quad (8a)$$

$$[G_2] \left\{ \frac{\partial \Phi^a}{\partial n} \right\} = [H_2] \{\Phi^a\} \quad (8b)$$

where $\{\Phi^a\}$, $\{\Phi^c\}$, and $\{\Phi^d\}$ represent potentials at the nodes on Γ_2 , Γ_1 , and Γ_0 , respectively. $[G_1]$ and $[H_1]$ are two $(N_L + N_B) \times (N_L + N_B)$ full matrices, and $[G_2]$ and $[H_2]$ are two $(N_L) \times (N_L)$ full matrices.

Since $\{\Phi^d\}$ is known as the Dirichlet boundary condition f imposed on Γ_0 , we rewrite (8a) as

$$[G'_1] \left\{ -\frac{\partial \Phi^c}{\partial n} \right\} = [H'_1] \{\Phi^c\} + \{b\} \quad (9)$$

where $[G'_1]$ and $[H'_1]$ are $N_L \times N_L$ two matrices of the corresponding upper left part of $[G_1]$ and $[H_1]$, and $\{b\}$ is an $N_L \times 1$ vector from the product of a partial matrix of $[H_1]$ and $\{\Phi^d\}$.

C. The FEM–BEM Coupling

Due to the coupling condition in (2), $\{\Phi^a\}$, $\{\Phi^c\}$ and their normal divergence on Γ_1 or Γ_2 are equivalent between the FEM and BEM. Thus, we can couple these systems of equations together. By multiplying the inverse matrices of $[G_2]$ and $[G'_1]$ to both sides of (9) and (8b), respectively, we obtain

$$\left\{ \frac{\partial \Phi^a}{\partial n} \right\} = [G_2]^{-1} [H_2] \{\Phi^a\} \quad (10a)$$

$$\left\{ \frac{\partial \Phi^c}{\partial n} \right\} = -[G'_1]^{-1} [H'_1] \{\Phi^c\} - [G'_1]^{-1} \{b\}. \quad (10b)$$

Apply (10) to (6), and move the corresponding parts from the right-hand side (RHS) to the left-hand side (LHS). Then, we obtain the final system of equations as (11)

$$\begin{bmatrix} A_{aa} - [T_2] [G_2]^{-1} [H_2] & A_{ab} & A_{ac} \\ A_{ba} & A_{bb} & A_{bc} \\ A_{ca} & A_{cb} & A_{cc} - [T_1] [G'_1]^{-1} [H'_1] \end{bmatrix} \times \begin{Bmatrix} \Phi^a \\ \Phi^b \\ \Phi^c \end{Bmatrix} = \begin{Bmatrix} 0 \\ 0 \\ [T_1] [G'_1]^{-1} \{b\} \end{Bmatrix}. \quad (11)$$

We, therefore, end up with the coupling between the FEM and BEM. After the system of equations are achieved, only $\{b\}$ on the RHS of (11) varies when the boundary condition on Γ_0 varies. It makes the coupling method efficient without computing the LHS of (11) again. The LHS of (11) is a sparse matrix containing two full square submatrices in the upper left and lower right parts. The preconditioned conjugate gradient method (PCGM) is used to solve the linear system of equations.

After solving (11) to get the potentials in Ω_1 and achieving the normal derivative of potential on Γ_0 , Γ_1 , and Γ_2 by (10), we can perform the boundary integration to get the potentials in Ω_0 and Ω_2 using Green's theorem

$$\Phi(\mathbf{r}) = \int_{\Gamma} K_2(\mathbf{r}, \mathbf{r}') \frac{\partial \Phi(\mathbf{r}')}{\partial n} dS(\mathbf{r}') - \int_{\Gamma} K_1(\mathbf{r}, \mathbf{r}') \Phi(\mathbf{r}') dS(\mathbf{r}'). \quad (12)$$

When the point $p(\mathbf{r})$ is far from either Γ_1 or Γ_2 , the seven-point Gaussian quadrature integration over each triangular element is performed. When $p(\mathbf{r})$ is close to Γ_1 or Γ_2 , the Duffy transform and a high-order Gaussian quadrature integration are performed to deal with the near singular integration. Meanwhile, when $p(\mathbf{r})$ is very near to either Γ_1 or Γ_2 , an extrapolation of the potentials in Ω_1 is used directly. Thus, all potentials in Ω are achieved.

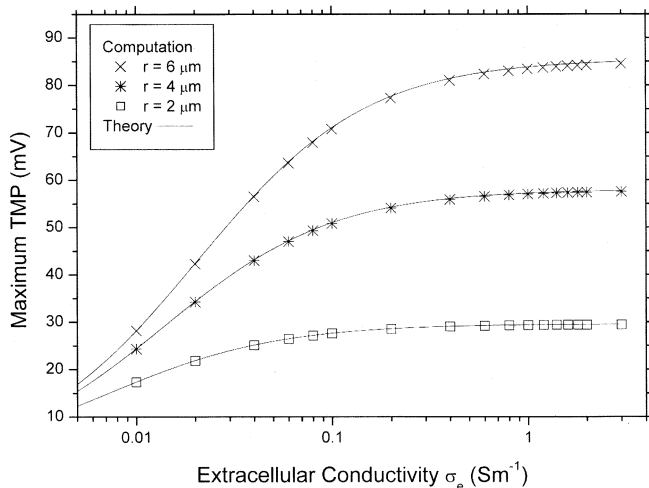


Fig. 4. Maximum TMP (both computed and theoretic) of a spherical “cell” of radius $2 \mu\text{m}$, $4 \mu\text{m}$, and $6 \mu\text{m}$ with different extracellular conductivity σ_e when the applied electric field is $100 \text{ V} \cdot \text{cm}^{-1}$.

IV. RESULTS

A. Verification

In order to verify the FEM–BEM coupling method, we compute the TMP on a spherical “cell” induced by a uniform field, where an analytical solution is known [5]. We take the membrane thickness to be 7 nm, and cell radii are 2, 4, and $6 \mu\text{m}$, respectively, the radius of Γ_0 being fixed at $40 \mu\text{m}$ (far enough from the cell). The intracellular conductivity is $\sigma_i = 0.5 \text{ S} \cdot \text{m}^{-1}$; the membrane conductivity is $\sigma_m = 5 \times 10^{-5} \text{ S} \cdot \text{m}^{-1}$; and the extracellular conductivity is taken from $\sigma_e = 0.01 \text{ S} \cdot \text{m}^{-1}$ to $\sigma_e = 3 \text{ S} \cdot \text{m}^{-1}$.

The mesh is achieved through the mapping technique as mentioned in Section II. There are 792 nodes and 1580 triangular elements on each layer between Γ_1 and Γ_2 , and 980 nodes and 1956 triangular elements on Γ_0 . Numerical results are shown in Fig. 4, where the intensity of the applied field is $100 \text{ V} \cdot \text{cm}^{-1}$. Relative errors of the computed maximum TMP are less than 1%. These numerical results show that the coupling method achieves an accurate result.

B. Maximum Induced TMP of an Erythrocyte

We use the geometric characteristics and conductivities defined in Section II to describe an erythrocyte, i.e., the membrane thickness is 7 nm, the intracellular conductivity is $\sigma_i = 0.8 \text{ S} \cdot \text{m}^{-1}$, and the membrane conductivity is $\sigma_m = 5 \times 10^{-5} \text{ S} \cdot \text{m}^{-1}$. Different extracellular conductivities σ_e are chosen to compare its effects on the induced TMP. The radius of spherical surface Γ_0 , which contains 980 nodes, is $40 \mu\text{m}$, and each layer between Γ_1 and Γ_2 contains 792 nodes.

When the electric field intensity is $100 \text{ V} \cdot \text{cm}^{-1}$, we compute the induced TMP of the erythrocyte by the coupling method. Fig. 5 shows the maximum induced TMP in different cases, while the electric field direction varies. When the erythrocyte is vertical to the electric field (the angle is $\pi/2$ in Fig. 5, and the direction of an erythrocyte is defined in Fig. 2), the maximum induced TMP is higher than the others. The maximum induced TMP in the vertical case is about 30% higher than the parallel

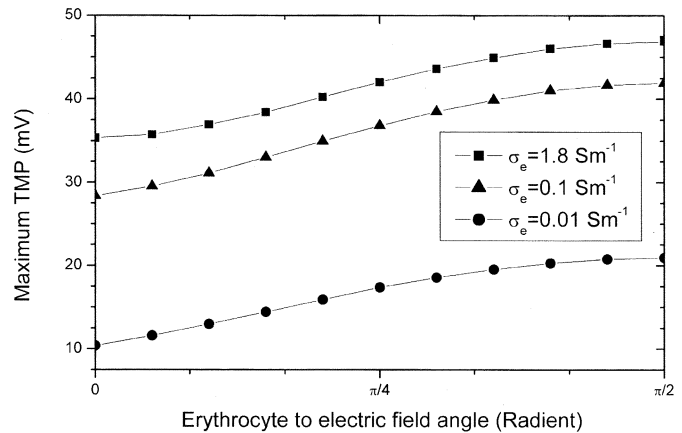


Fig. 5. The maximum induced TMP of an erythrocyte in the electric field with intensity of $100 \text{ V} \cdot \text{cm}^{-1}$, when the extracellular conductivity σ_e is $1.8 \text{ S} \cdot \text{m}^{-1}$, $0.1 \text{ S} \cdot \text{m}^{-1}$, and $0.01 \text{ S} \cdot \text{m}^{-1}$, respectively. Here, x shows the angle between the erythrocyte and the electric field.

case. Moreover, the higher the extracellular conductivity is, the larger the maximum induced TMP is.

Fig. 6 shows equipotential lines around the erythrocyte when the electric field’s direction varies. Fig. 7 shows the induced TMP on the line $x = 0$ of the erythrocyte surface. From these figures, it is interesting to notice where the maximum induced TMP is located. When the erythrocyte is parallel to the electric field (angle θ is zero), the maximum induced TMP is located at the center of the biconcave instead of at the convex region. Furthermore, in this case a large area on the erythrocyte surface is at a high induced TMP (i.e., the area with TMP above 25 mV). When the erythrocyte direction is vertical to electric field, maximum TMP reaches the highest value (about 45 mV). However, the area with high induced TMP is smaller compared to the others.

V. DISCUSSION

For the spherical “cell” model, the FEM–BEM coupling method gives an accurate numerical result. Potential errors at nodes are less than 0.5 mV, which may guarantee that the error of the maximum induced TMP is less than 1%. The high accuracy seems beneficial due to the characteristics of the BEM, since the errors of potentials and potential divergence are at the same order in the numerical results from the BEM.

The membrane electric breakdown occurs when the TMP is above 500 mV. Thus, the electric field intensity threshold based on our computation is estimated. When $\sigma_e = 1.8 \text{ S} \cdot \text{m}^{-1}$, it can be found that the threshold is about $1100 \text{ V} \cdot \text{cm}^{-1}$, which agrees with the experiments on erythrocyte electroporation.

We compare the maximum induced TMP of an erythrocyte with a long axis of $4 \mu\text{m}$ and a spherical “cell” with radius of $4 \mu\text{m}$, when an extracellular conductivity σ_e is $1.8 \text{ S} \cdot \text{m}^{-1}$ and the electric field is $100 \text{ V} \cdot \text{cm}^{-1}$. The maximum induced TMP on the erythrocyte is 46 mV, which is about 20% less than the maximum induced TMP of the spherical cell — 57 mV. Therefore, the spherical “cell” model seems to be an efficient way to estimate the maximum induced TMP.

When the erythrocyte is parallel to the electric field, the maximum TMP appears at the center of the erythrocyte, and a large

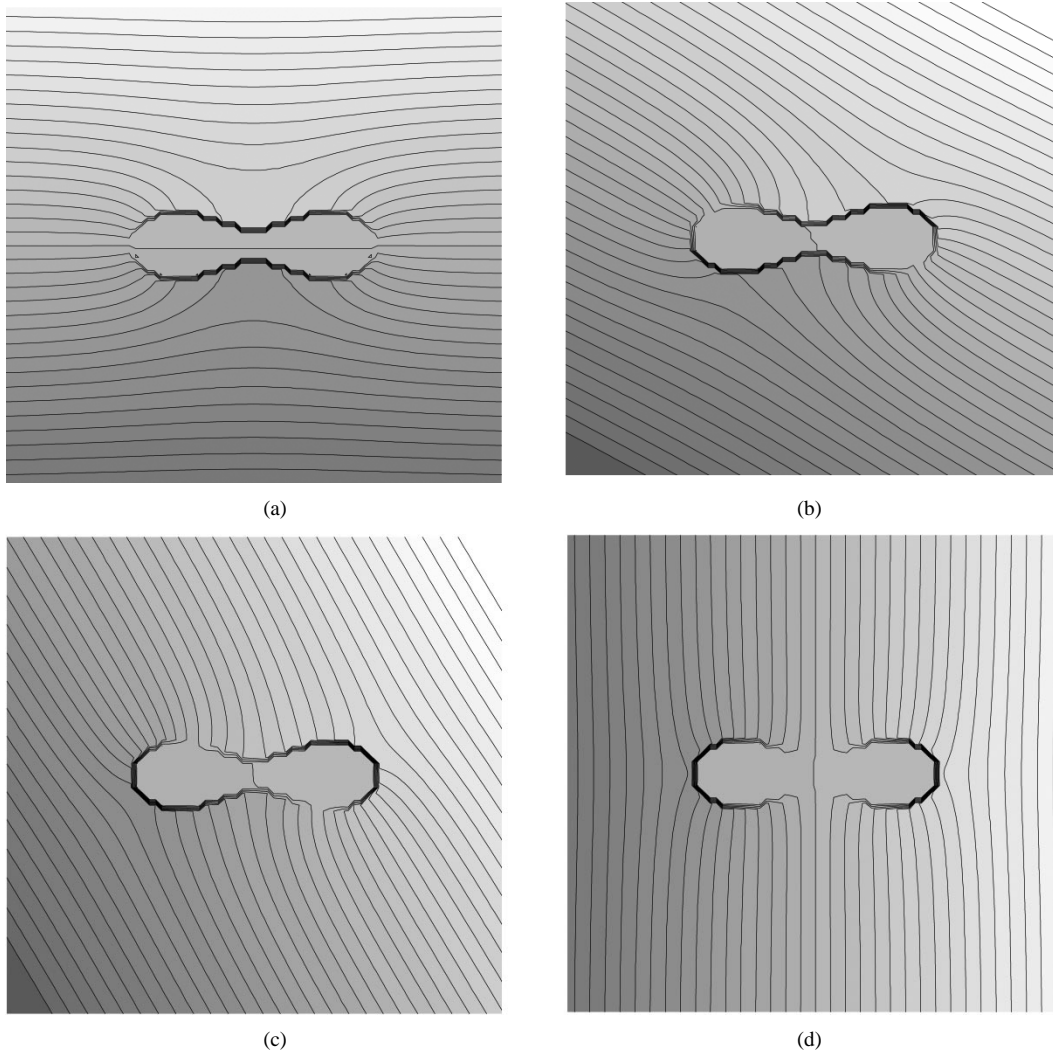


Fig. 6. Equipotentials around an erythrocyte (a cross section of YOZ) when the direction of applied electric field \mathbf{E} is changed from $-\mathbf{z}$ to $-\mathbf{y}$ (angle θ between erythrocyte and the electric field is zero, $\pi/6$, $\pi/3$, and $\pi/2$ respectively). $|E| = 100 \text{ V} \cdot \text{cm}^{-1}$, and $\sigma_e = 1.8 \text{ S} \cdot \text{m}^{-1}$. The potential difference between each two adjacent equipotentials is 5 mV.

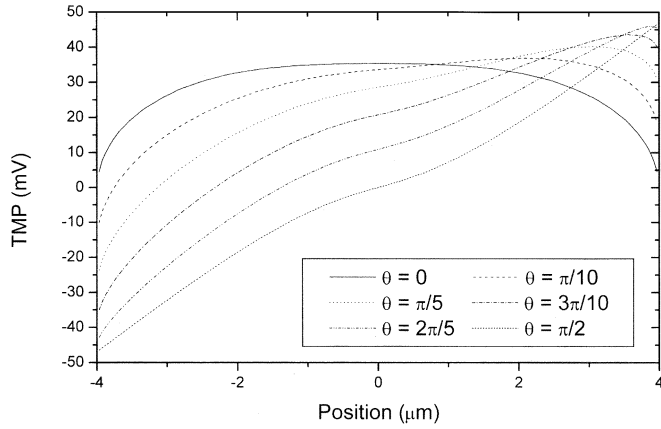


Fig. 7. TMP on the erythrocyte surface ($x = 0$ and $z > 0$), when an applied electric field \mathbf{E} varies from $-\mathbf{z}$ to $-\mathbf{y}$. $\sigma_e = 1.8 \text{ S} \cdot \text{m}^{-1}$, and $|E| = 100 \text{ V} \cdot \text{cm}^{-1}$.

area of the erythrocyte is exposed in a high TMP range. It may be a reason that pores are often generated at the center of erythrocytes in some bioelectromagnetic experiments.

The FEM–BEM coupling method owns some advantages on computing the induced TMP of biological cells. Since the membrane is a thin shell at nanometer scale, one surface mesh, which is extended to a 3-D mesh, is used to describe the membrane, as discussed in Section II. Moreover, in Ω_0 and Ω_2 , only surface meshes are required, since the BEM is applied. Thus, it is convenient to adopt the mesh generation. Moreover, once the mesh is generated and the inverse matrices revolved in the BEM are achieved, only the final system equations, as (11), are required to solve when the Dirichlet boundary condition is changed, i.e., to compute different electric fields.

The FEM–BEM coupling method is applicable to other biological cells smoothly, or to some microstructures at nanometer scale in a large space. Since the membrane is inside the FEM computational domain, it is convenient to change its conductivity or add another microstructure, such as a pore. Then, the potential distribution with the presentation of a pore may also be achieved.

In this paper, we assume the erythrocytes are far away from each other. In fact, we may put two or more erythrocytes near each other. Then, we use the FEM–BEM coupling method to

study the interaction between them, such as forces between them, maximum TMP variations due to other near erythrocytes, and so on.

When an electromagnetic pulse is applied, a time domain problem should be solved. We may extend this coupling method to deal with the finite volume time domain method [15] and the BEM in time domain to study the induced TMP. Further study on the time domain problem is required.

REFERENCES

- [1] J. C. Weaver and Y. A. Chizmadzdev, "Theory of electroporation: A review," *Bioelectrochem. Bioenerg.*, vol. 41, pp. 135–160, 1996.
- [2] C. Liu *et al.*, "Cell deformation and increase of cytotoxicity of anti-cancer drugs due to low-intensity transient electromagnetic pulses," *IEEE Trans. Plasma Sci.*, vol. 28, pp. 150–154, Feb. 2000.
- [3] U. Zimmermann, "Electric field-mediated fusion and related electrical phenomena," *Biochem. Biophys. Acta*, vol. 694, pp. 227–277, 1982.
- [4] E. C. Fear and M. A. Stuchly, "Biological cells with gap junctions in low-frequency electric fields," *IEEE Trans. Biomed. Eng.*, vol. 45, pp. 856–866, July 1998.
- [5] C. E. Miller and C. S. Henriquez, "Three-dimensional finite element solution for biopotentials: Erythrocyte in an applied field," *IEEE Trans. Biomed. Eng.*, vol. 35, pp. 712–718, Sept. 1988.
- [6] G. Bartsch, M. Baumann, and R. Grebe, "Numerical calculation of electric fields surrounding biological cells in three dimensions," *Bioelectrochem. Bioenerg.*, vol. 42, pp. 221–226, 1997.
- [7] J. Jin, *Finite Element Method in Electromagnetics*. New York: Wiley, 1993.
- [8] J. Douglas Jr., J. E. Santos, and D. Sheen, "A nonconforming mixed finite element method for Maxwell's equations," *Math. Models Methods Appl. Sci.*, vol. 10, pp. 593–613, 2000.
- [9] A. A. Becker, *The Boundary Element Method in Engineering*. New York: McGraw-Hill, 1992.
- [10] P. K. Kythe, *An Introduction to Boundary Element Methods*. Boca Raton, FL: CRC, 1995.
- [11] G. C. Hsiao, "The coupling of boundary element and finite element methods," *Z. Angew. Math. Mech.*, vol. 70, pp. 493–503, 1990.
- [12] C. Johnson and J. C. Nedelec, "On the 'Coupling of boundary integral and finite element methods,'" *Math. Comput.*, vol. 35, pp. 1063–1080, 1980.
- [13] F. Bordi, C. Cametti, and T. Gili, "Dielectric spectroscopy of erythrocyte cell suspensions. A comparison between Looyenga and Maxwell–Wagner–Hnai effective medium theory formulations," *J. Non-Cryst. Solids*, vol. 305, pp. 278–284, 2002.
- [14] P. W. Kuchel and E. D. Fackerell, "Parametric-equation representation of biconcave erythrocytes," *Bull. Math. Biol.*, vol. 61, pp. 209–220, 1999.
- [15] C. D. Munz, R. Schneider, and U. Vob, "A finite-volume method for the Maxwell equations in the time domain," *SIAM J. Sci. Comput.*, vol. 22, pp. 449–475, 2000.

Changjun Liu was born on April 18, 1973, in Hebei, China. He received the B.S. degree from Hebei University, Hebei, China, in 1994 and the M.S. and Ph.D. degrees from Sichuan University, Chengdu, China, in 1997 and 2000, respectively.

From 2001 to 2002, he was a Postdoc at Seoul National University, Seoul, Korea. He is currently an Associate Professor in the College of Electronics and Information Science, Sichuan University. His research interests include numerical methods on electromagnetics and bioelectromagnetics.

Dr. Liu is a Senior Member of the Chinese Institute of Electronics.

Dongwoo Sheen was born on April 21, 1957, in Kyungki, Korea. He received the B.S. and M.S. degrees from Seoul National University, Seoul, Korea, in 1981 and 1983, respectively, and the Ph.D. degree in mathematics from Purdue University, West Lafayette, IN, 1991.

From 1991 to 1992, he was a Visiting Professor at Istituto di Analisi Numerica, Pavia, Italy. From 1992 to 1993, he was a Postdoc at Purdue University. His research interests include numerical analysis, especially on DDM and non-conforming FEM.

Kama Huang received the M.S. and Ph.D. degrees in microwave theory and technology from the University of Electronic Science and Technology, Chengdu, China in 1988 and 1991, respectively.

Since 1994, he has been a Professor, Department of Radio and Electronics, Sichuan University, Chengdu, China, and the Director of the department since 1997. His research interests include the interaction between electromagnetic fields and complex media in biological structure and reaction systems.